Development and validation of a wear prediction model for railway applications including track flexibility

Wear 486–487 (2021) 204092

Contents lists available at ScienceDirect

Wear

journal homepage: www.elsevier.com/locate/wear

Development and validation of a wear prediction model for railway applications including track flexibility

Zhiyong Shi [a], Shengyang Zhu [b], Andrea Rindi [a], Enrico Meli [a,*]

[a] Department of Industrial Engineering, University of Florence, Via S. Marta n. 3, 50139 Firenze, Italy
[b] State Key Laboratory of Traction Power, Southwest Jiaotong University, Chengdu, Sichuan, China

ARTICLE INFO

Keywords:
Wheel–rail wear
Track flexibility
Wheel–rail contact
Vehicle–track interaction
Prediction model

ABSTRACT

The simultaneous prediction of wheel surface wear is one of the most challenging tasks in the railway field, which requires the knowledge of vehicle–track dynamics, rolling contact mechanics, and other tribological phenomena. In this paper, a new model for predicting wheel profile wear is presented to study in detail the characteristics of wear in the railway. The model is able to consider the effect of track flexibility on wheel wear evolution. The proposed modelling approach includes a vehicle–track coupled model for vehicle dynamical simulation, the local contact model for wheel–rail interaction, and an energetic approach for surface wear evaluation. The whole model has been validated by the comparison with experimental data coming from Chinese high-speed railway lines. The results show that the new model assures high computational efficiency as well as reaches a good prediction accuracy. The proposed model allows the investigation of the role played by different track parameters related to track flexibility on the wheel and rail wear evolution. The influence of the fastener and railpad stiffness on the wheel wear evolution is presented, using the proposed model.

1. Introduction

Wear at wheel–rail contact interface is one of the most fundamental research in the railway field. It alters the profiles for both rail and wheel, influences the interaction of wheel and rail and further threatens the running performance of the vehicle and the service performance of the track in the long-term run. In the past years, vehicle dynamics, contact mechanics, and tribology based research has intensively promoted the understanding of wear in wheel–rail contact and dynamic models to predict the evolution. To predict the wear evolution between the wheel–rail interface, a general model is demanded to include the dynamics simulation and the wear evaluation. Both the vehicle–track dynamics model and the wear evaluation model affect the accuracy and efficiency of the prediction model remarkably.

Early study on wear modelling dates back to the 1950s when Archard [1] experimentally revealed that the wear rate is proportional to the load, which has been widely developed and utilized as the Archard model among researchers [2]. Pearce and Sherratt [3] proposed the BRR (British Railway Research) model, which starts by calculating the global contact forces and creepages acting on the contact patch, and a defined wear index is applied for evaluating the amount of worn material. After that, Zobory [4] proposed the Zobory model, which has introduced a stochastic energy flow density as a wear index related to the tangential stress and sliding velocity. The KTH model [5,6], was developed basing on Archard's model, assuming the wear amount proportional to the product of normal force and sliding distance. Extended research also includes more measurement results [7], which consider the local contribution of elastic deformation by modifying a sliding velocity calculation method. The USFD model, is came up based on plentiful twin-disc tests [8–10]. The wear characteristics are investigated among different materials, different environmental conditions, with stable control for slip and contact pressure settings. Wear regimes and transitions has been identified using the maps. The map describes wear rate as a function of wear index, which includes mild, severe and catastrophic [9]. Comparative study on different wear evaluation models can be found in [11–13].

Based on the above wear models, many researches predicting wear in the railway field have been performed in recent years [14,15]. Jin et al. [16] conducted a series of wear investigations on rail and wheel of both high speed and heavy haul railway lines [17–19]. A model consisting of two interactive parts was developed by Ignesti et al. [20], which includes vehicle model part for dynamical analysis and damage model part for wear estimation.

Most of the existing models for wheel and rail wear estimations did not consider the influence from the track part sufficiently. The track models were sometimes quite simple (due to using commercial codes), that ignored the elastic deformation of the track structure. The flexible

* Corresponding author.
E-mail addresses: zhiyong.shi@unifi.it (Z. Shi), syzhu@swjtu.edu.cn (S. Zhu), andrea.rindi@unifi.it (A. Rindi), enrico.meli@unifi.it (E. Meli).

https://doi.org/10.1016/j.wear.2021.204092
Received 19 February 2021; Received in revised form 21 August 2021; Accepted 1 September 2021
Available online 8 September 2021

deformation of the track structure has a significant influence on the creepages/creep-forces between wheel and rail and therefore influences greatly on the friction work and wear of the wheel/rail surfaces. Aceituno et al. [21] presented a comparison between rigid track and flexible track affecting wheel wear. Tao et al. [22] compared different track models and discussed the influence of track modelling on wear of wheel, from the choice with or without track flexibility and different updating strategy. Kaiser et al. [23] investigated the combination of the flexibilities of the wheelsets and the track impacting on the wheel–rail contact, by the integration of the wheel–rail contact into the vehicle–track model, using floating frame of reference formulation describing the kinematics.

However, the quantitative discussion of the track flexibility lacked in-depth analysis. Therefore, a wear prediction model able to consider the effect of track flexibility on wear evolution and a detailed investigation on revealing different track parameters affecting the wear evolution have been attempted by the authors. To identify the track flexibility, the present work is focused on the variation of the fastener and railpad stiffness, which has been found affecting the wheel–rail force remarkably [24].

This paper firstly presents the numerical model that considers the evolution of wheel profile, and then validates this model by experimental results. Further, it investigates the influence of the fastener and railpad stiffness on wheel wear evolution, as the fastener and railpad is closely connected with the wheel–rail contact force. The methodology of the study and the model description is detailed in Section 2. Then the results are compared with experimental data coming from Chinese high speed railway lines for validation in Section 3. After the validation of the model, the influence of fastener and railpad stiffness on wheel wear evolution is investigated. The results disclosed the important connection between railpad stiffness and the wear evolution, through the wheel–rail contact forces and locations.

2. Methodology

2.1. General architecture

The general architecture of the integrated model is shown in Fig. 1. As it depicts, two main parts are included, the dynamics model and the wear model. Inside the dynamics model, to obtain the contact variables, kinematic variables, contact points and forces are transferred to the global contact model. Based on the results from the dynamics model, the local contact variables can be obtained and then further passed to wear evaluation model. The wear evaluation model estimates the removed material from the profiles of the wheel and rail. After obtaining the removed material, the profiles are updated, generating new profiles, which become the new input profiles for vehicle–track coupled model.

2.2. Vehicle–track coupled model

The dynamics model is based on the theory of vehicle–track coupled dynamics [25,26], which includes a MBS vehicle model, and a multi-layers track model. The global wheel–rail contact model used the trace curve method [27] to detect the location of contact points. And the non-linear Hertzian elastic contact theory is used to calculate the wheel–rail normal contact forces. The tangential wheel–rail contact force is calculated by the Kalker's linear creep theory [28] and then modified by the Shen–Hedrick–Elkins non-linear model [29].

Fig. 2 illustrates the coupled dynamic model of the vehicle and the slab track. The vehicle is modelled as a rigid multibody model, which includes a carbody, two double-axle bogies, the primary suspension system and the secondary suspension systems. Each component of the vehicle has five degrees of freedom (DOFs): the vertical displacement Z, the lateral displacement Y, the roll angle Φ, the yaw angle Ψ, and the pitch angle β. The total DOFs of the vehicle is listed in Table 1.

Table 1
Degrees of freedom for the vehicle model.

Vehicle component	Lateral	Vertical	Roll	Yaw	Pitch
Wheelset1	Y_{w1}	Z_{w1}	Φ_{w1}	Ψ_{w1}	β_{w1}
Wheelset2	Y_{w2}	Z_{w2}	Φ_{w2}	Ψ_{w2}	β_{w2}
Wheelset3	Y_{w3}	Z_{w3}	Φ_{w3}	Ψ_{w3}	β_{w3}
Wheelset4	Y_{w4}	Z_{w4}	Φ_{w4}	Ψ_{w4}	β_{w4}
Front bogie frame	Y_{b1}	Z_{b1}	Φ_{b1}	Ψ_{b1}	β_{b1}
Rear bogie frame	Y_{b2}	Z_{b2}	Φ_{b2}	Ψ_{b2}	β_{b2}
Carbody	Y_c	Z_c	Φ_c	Ψ_c	β_c

The equations of motion for the vehicle can be written as:

$$\mathbf{M}_v\mathbf{A}_v + \mathbf{C}_v(\mathbf{V}_v)\mathbf{V}_v + \mathbf{K}_v(\mathbf{X}_v)\mathbf{X}_v = \mathbf{F}_v(\mathbf{X}_v, \mathbf{V}_v, \mathbf{X}_t, \mathbf{V}_t) \tag{1}$$

where $\mathbf{M}_v$ is the mass matrix of the vehicle, $\mathbf{C}_v(\mathbf{V}_v)$ and $\mathbf{K}_v(\mathbf{X}_v)$ are the stiffness and damping matrix of the vehicle, which can depend on the current state of the vehicle subsystem to describe nonlinearities within the suspension. $\mathbf{A}_v$, $\mathbf{V}_v$, and $\mathbf{X}_v$ are the vectors of the accelerations, velocities and displacements of the vehicle subsystem; $\mathbf{V}_t$, and $\mathbf{X}_t$ are the velocities and displacements of the track subsystem. $\mathbf{F}_v$ is the load vector representing the non-linear wheel–rail contact forces, which is the function of the motions $\mathbf{V}_v$, and $\mathbf{X}_v$ of the vehicle and $\mathbf{V}_t$, and $\mathbf{X}_t$ of the track.

For the modelling of the track system, the rail, the slab, the concrete bases, the supporting fasteners/rail pads and the connected CAM layers are included. The rail is treated as a Euler–Bernoulli beam resting on rail pads, and the vertical, lateral, and torsional motions of the rails are taken into consideration. The slab and concrete base of the slab track are described as elastic rectangle plates supported on viscoelastic foundation in the vertical direction, while only the rigid mode of the vibrations in the lateral direction is considered due to the large lateral bending stiffness. As shown in Fig. 2, the three layers of discrete springs and dampers represent the elasticity and damping effects of the rail fastener, the CA mortar layer and the subgrade, respectively. The equations of the motions of each component and solutions to the equations can be referred in [25,26].

The global contact model used the trace curve method to detect the location of wheel–rail contact points [27]. And the non-linear Hertzian elastic contact theory is used to calculate the wheel–rail normal contact forces [28,29].

$$P_N(t) = \left[\frac{1}{G}\delta N(t)\right]^{3/2} \tag{2}$$

where G represents the wheel–rail contact constant, and $\delta N(t)$ is the normal compressing deformation at wheel–rail contact point. The left and right wheel–rail normal compressing deformation can be expressed as:

$$\begin{cases} \delta N_L = \frac{\delta Z_L}{cos(\delta_L + \phi_w)} \\ \delta N_R = \frac{\delta Z_R}{cos(\delta_R - \phi_w)} \end{cases} \tag{3}$$

where δ_L and δ_R refer to the wheel–rail contact angles for left and right side. δZ_L and δZ_R are the left and right wheel–rail vertical relative displacements. The tangential wheel–rail contact force is calculated by the Kalker's linear creep theory [28] and then modified by the Shen–Hedrick–Elkins non-linear model [29].

$$\begin{cases} F_x = & -f_{11}\varepsilon_x \\ F_y = & -f_{22}\varepsilon_y - f_{23}\varepsilon_{sp} \\ M_z = & -f_{22}\varepsilon_y - f_{33}\varepsilon_{sp} \end{cases} \tag{4}$$

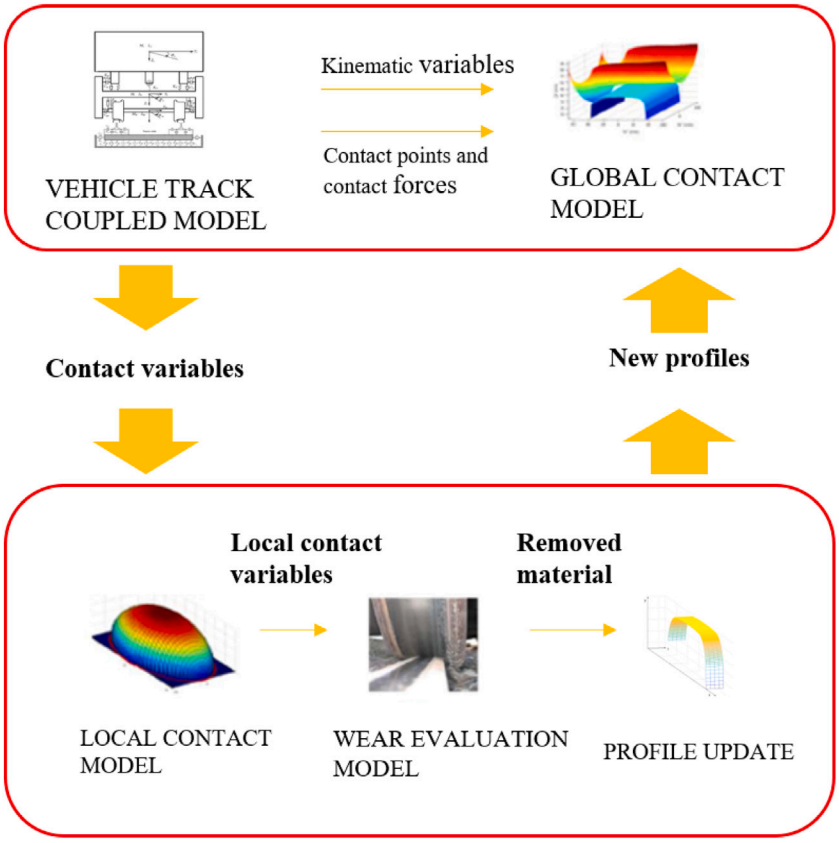

Fig. 1. A general architecture of wear prediction model.

$$\begin{cases} F_x' = \frac{F}{F'} F_x \\ F_y' = \frac{F}{F'} F_y \\ M_z' = \frac{F}{F'} M_z \end{cases} \tag{5}$$

while

$$F = \sqrt{F_x^2 + F_y^2}$$

$$F' = \begin{cases} \mu N \left[\frac{F}{\mu N} - \frac{1}{3} (\frac{F}{\mu N})^2 + \frac{1}{27} (\frac{F}{\mu N})^3 \right] & \text{for} \quad (F \le 3\mu N) \\ \mu N & \text{for} \quad (F > 3\mu N) \end{cases}$$

where F_x, F_y and M_z are the longitudinal, lateral creep forces and creep torque before non-linear modification. f_{ij} represents the creep coefficients. ε_x, ε_y and ε_{sp} are the longitudinal, lateral and spin creepage. F_x', F_y' and M_z' are the modified longitudinal, lateral creep forces and creep torque. μ is the wheel–rail contact friction coefficient.

2.3. Local wheel–rail contact model

The local contact model is designed to calculate the local contact variables including the tangential contact pressures $\vec{p}_t$ and local sliding velocity $\vec{s}$, and the corresponding normal pressure $\vec{p}_n$, the contact points $\vec{P}_{cw}$, and the wheel kinematic variables. A reference system is defined at the wheel–rail interface on the contact plane. Fig. 3 illustrates the x, y and z axes being the longitudinal, the transversal and the normal directions of the contact area.

The semi-axes a and b of the elliptical patch can be discretized in a bi-dimensional grid, where b is the transversal axis with respect to the motion direction, and a is the longitudinal axis along the motion direction, so that the grid resolution will be non-constant, as following.

$$\Delta y = \frac{2b}{n_y - 1} \tag{6}$$

In Eq. (6), the transversal axis is divided in $n_y - 1$ equal parts of magnitude Δy by means of n_y equidistant nodes. Since the discretion in the longitudinal axis is geometric dependent on the transversal axis, the discretion can be achieved by means of n_x equidistant nodes into $n_x - 1$ equal parts, as

$$\Delta x(y) = \frac{2a(y)}{n_x - 1} \tag{7}$$

$$a(y) = a\sqrt{1 - \frac{y^2}{b^2}} \tag{8}$$

Based on the theory of FASTSIM [31] and Polach [32], the flexibility coefficient L is introduced. Thus the relationship between the tangential elastic displacements $\vec{u}$ and the tangential pressure $\vec{p}_t$ is approximated, saving the computation efforts. The relationship can be expressed as,

$$\vec{u}(x, y) = L\vec{p}_t(x, y) \tag{9}$$

while

$$L = L(\varepsilon, a, b, G, \upsilon) \tag{10}$$

where ε is the global rigid creepages, G is the wheel and rail combined shear modulus, and υ is the wheel and rail combined Poisson's ratio. L, as a function of ε, a, b, G and υ, can be written as,

$$L = \frac{|\varepsilon_x| L_1 + |\varepsilon_y| L_2 + c |\varepsilon_{sp}| L_3}{(\varepsilon_x^2 + \varepsilon_y^2 + c^2 \varepsilon_{sp}^2)^{1/2}} \tag{11}$$

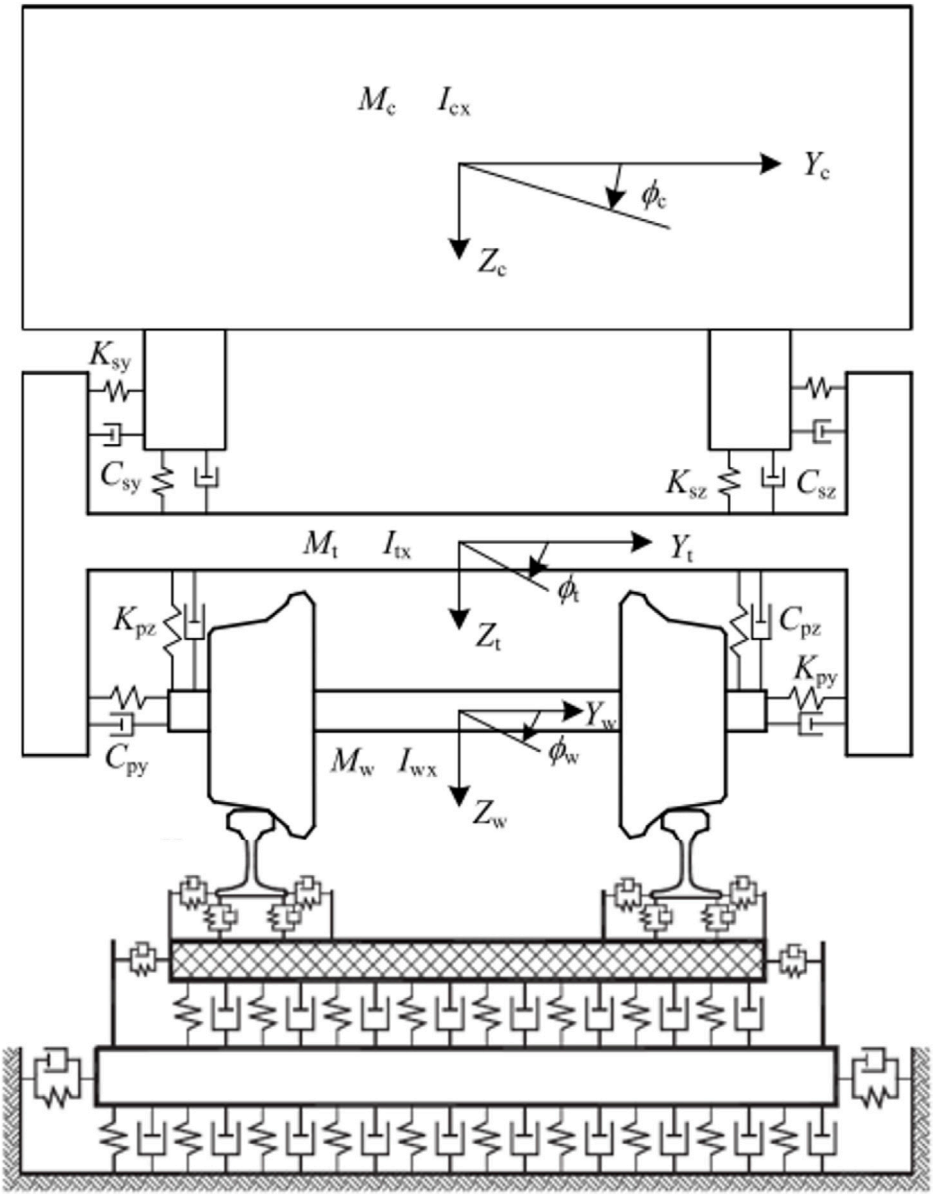

Fig. 2. Coupled dynamic model of a vehicle and a slab track [30].

while

$$\vec{v}_{pc} = (v_{pcx}, v_{pcy}) = \vec{v}_{\omega} + \vec{\omega}_w \times (\vec{P}_c - \vec{G}_w)$$

$$\varepsilon_x = \frac{v_{pcx}}{\|\vec{v}_w\|}$$

$$\varepsilon_y = \frac{v_{pcy}}{\|\vec{v}_w\|}$$

$$\varepsilon_{sp} = \frac{\vec{\omega}_w \vec{n}}{\|\vec{v}_w\|}$$

$$L_1 = \frac{8a}{3GC_{11}}$$

$$L_2 = \frac{8a}{3GC_{22}}$$

$$L_3 = \frac{\pi a^2}{4GC_{23}}$$

$$c = \sqrt{ab}$$

where $\vec{v}_{pc}$ is the velocity of the contact point rigidly connected to the wheel, and $\vec{v}_{\omega}$ is the wheel velocity, $\vec{\omega}_w$ is the wheel angular velocity, $\vec{P}_c$ is the contact point, $\vec{G}_w$ is the wheel position, and $\vec{n}$ is the outgoing normal unit vector of the wheel surface. C_{ij}, the constants, are functions of Poison's ratio υ and the ratio of ellipse semi-axes a and b, and can be found in [31]. As the local slip velocity can be achieved by derivation considering the elastic local displacement and the rigid ones:

$$\vec{s}(x, y) = \vec{u}(x, y) + V \begin{bmatrix} e_x \\ e_y \end{bmatrix} \tag{12}$$

with

$$\begin{bmatrix} e_x \\ e_y \end{bmatrix} = \begin{bmatrix} \varepsilon_x - y_j \varepsilon_{sp} \\ \varepsilon_y - x_i \varepsilon_{sp} \end{bmatrix} \tag{13}$$

where $V = \|\vec{v}_w\|$ is the longitudinal vehicle speed, and ε_x, ε_y are the rigid local creepages. The normal contact pressure for the generic point of the grid with (x_i, y_j) can be expressed as

$$p_n(x_i, y_i) = \frac{3}{2} \frac{N_c}{\pi ab} \sqrt{1 - \frac{x_i^2}{a^2} - \frac{y_j^2}{b^2}} \tag{14}$$

where N_c is the normal force, while the limit adhesion pressure $\vec{p}_A$ is:

$$\vec{p}_A(x_i, y_i) = \vec{p}_i(x_{i-1}, y_j) - \begin{bmatrix} e_x \\ e_y \end{bmatrix} \frac{\Delta x(y_i)}{L} \tag{15}$$

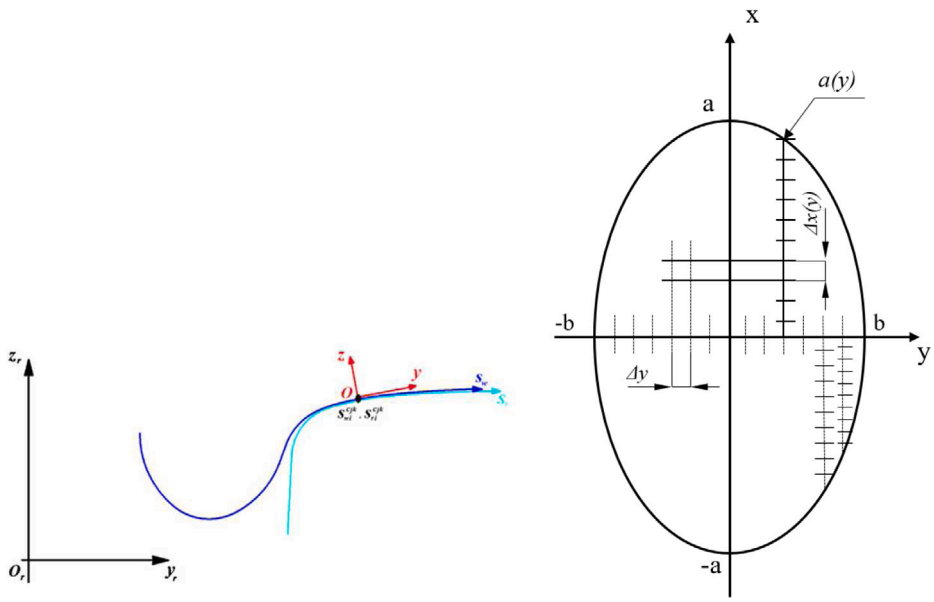

(a) x, y and z axes of the contact interface (b) Contact patch discretization

Fig. 3. The reference system at the wheel–rail interface.

The calculation of point (x_i, y_j) will pass from the point (x_{i-1}, y_j) by Eq. (16)

$$\begin{aligned}
&if \left\|\vec{p}_A(x_i, y_j)\right\| \le \mu(x_i, y_j) p_n(x_i, y_j) \\
&\quad \begin{cases} \vec{p}_t(x_i, y_j) = \vec{p}_A(x_i, y_j) \\ \vec{s}(x_i, y_j) = 0 \end{cases} \\
&if \left\|\vec{p}_A(x_i, y_j)\right\| > \mu(x_i, y_j) p_n(x_i, y_j) \\
&\quad \begin{cases} \vec{p}_t(x_i, y_i) = \mu(x_i, y_i)\vec{p}_n(x_i, y_i)\frac{\vec{p}_A(x_i, y_i)}{\left\|\vec{p}_A(x_i, y_i)\right\|} \\ \vec{s}(x_i, y_i) = \frac{LV}{\Delta x(y_j)}[\vec{p}_t(x_i, y_i) - \vec{p}_A(x_i, y_i)] \end{cases}
\end{aligned} \tag{16}$$

where $\mu(x_i, y_j)$ is the friction coefficient. In this paper, we assume $\mu(x_i, y_j)$ being constant as 0.35 for all points in the contact patch, while the discussion for a varying $\mu(x_i, y_j)$ can be referred in [33]. Assuming the boundary conditions that the stresses and slip velocity out of the contact patch are set to zero, namely, $\vec{p}_t(x_1, y_j) = \vec{0}$ and $\vec{s}(x_1, y_j) = \vec{0}$ for $1 \le j \le n_y$, the desired distribution of $p_n(x_i, y_j)$, $\vec{p}_t(x_i, y_j)$ and $\vec{s}(x_1, y_j)$ can be determined by iterating for $2 \le i \le n_x$ and $1 \le j \le n_y$.

2.4. Wear evaluation model

The wear calculation model is based on the energy transfer method, which assumes the material loss as a function of the energy dissipated at the contact patch, as referred in [34]. Assuming that wear rate is related to work done at the wheel–rail contact, namely the product of the individual creep forces, T, and creepages, γ. Define $T\gamma/A$ as wear index I_w, where A is the contact patch area. Consider one cell of the discretized patch, as:

$$\gamma(x, y) = \frac{\vec{s}(x, y)}{V} \tag{17}$$

where $\vec{s}(x, y)$ represents the slip velocity, and the V is the longitudinal vehicle speed, we obtain:

$$I_w = \frac{T\gamma(x, y)}{A} = \frac{\vec{p}_t \cdot \vec{s}(x, y)}{V} \tag{18}$$

Eq. (18) can be solved by previous determined results. Note that wear occurs only in the slip region of the contact patch. Define the wear rate as K_w, the relationship between the wear rate and the factor $T\gamma/A$ is obtained from experimental tests. Here, we refer [34], in the case of R8T steel for the wheel and UIC60 900 A for the rail, the wear rate can be expressed as:

$$K_w\left(I_w\right) = \begin{cases} 5.3 I_w & I_w < 10.4 \\ 55.1 & 10.4 \le I_w \le 77.2 \\ 61.9 I_w - 4778.7 & I_w > 77.2 \end{cases} \tag{19}$$

Note that the units of wear rate here are mg/mm^2/km. Given the wear rate from Eq. (19), the volume of removed material on the wheel, for unit of distance travelled by the vehicle can be calculated as:

$$\delta^{jk}_{P_{wi(t)}}(x, y) = K_w\left(I_w\right)\frac{1}{\rho} \tag{20}$$

where $\delta^{jk}_{P_{wi(t)}}$ represents the wear depth distributions for the ith contact patch of the jth wheel during the kth of the total dynamical simulations and ρ is the density of the material.

2.5. Profile updating strategy

After we obtain the amount of worn material for the profiles at each step, the result will be transferred as inputs for the next step in a loop strategy, so as to achieve an updated profile.

The update strategy includes following operations:

- For each contact step, get the spatial integration of all the wear contributions inside the contact patch, along the longitudinal direction and then get the average value per unit length. In this procedure, we study the contact patch at each time step, and assume that the wear effect of contact at each time step on the wheel surface is equal.
- During a certain time series of simulation, sum all the wear contributions coming from all time-steps to obtain the depth of the removed material from the wheel. For one time point among the time series, sum the wear contributions coming from all the contact points of a contact pair.
- Amplify the removed material during the dynamic simulations to reduce the simulated track length through a scaling procedure.
- A smoothing procedure is adopted to remove the numerical noise.

The longitudinal integration at each contact path:

$$\delta^{tot}_{P^{jk}_{wi}}(y) = \frac{1}{2\pi w_{y^{jk}_{wi}}}\int_{-a(y)}^{+a(y)} \delta_{P^{jk}_{wi}}(x, y)\,\mathrm{d}x \tag{21}$$

Fig. 4. Discretization of the total mileage.

where $\delta^{tot}_{P^{jk}_{wi}}$ represents the accumulated wear distribution along x direction for the wheel, the $w_{y^{jk}_{wi}}$ is the radius of the wheel at y^{jk}_{wi}. After obtaining the accumulated wear distribution along x direction for the wheel in Eq. (21), we sum all the contributions from each simulation time step by track integration. As y can be transformed as following, referring Fig. 3:

$$y \approx s_w - s^{cjk}_{wi} \tag{22}$$

$$w(y_w) = w\left(y_w\left(s_w\right)\right) = \widetilde{w}(s_w) \tag{23}$$

where y stands for the local contact coordinates; s_w is the natural coordinates for the wheel; s^{cjk}_{wi} is the natural abscissas of the ith contact points, which can be evaluated from their positions P^{jk}_{wi}; $w(y_w)$ is the curve of the contact points on wheel and rail. Therefore, the track integration leads to:

$$\begin{aligned} \Delta_{P^{jk}_{wi}}(y) &= \int_{T_{in}}^{T_{end}} \delta^{tot}_{P^{jk}_{wi}(t)}(y)\, V(t)\mathrm{d}x \\ &\approx \int_{T_{in}}^{T_{end}} \delta^{tot}_{P^{jk}_{wi}(t)}\left(s_w - s^{cjk}_{wi}\right) V(t)\mathrm{d}x = \Delta_{P^{jk}_{wi}}(s_w) \end{aligned} \tag{24}$$

where $\Delta_{P^{jk}_{wi}}(s_w)$ is the depth of the removed material from the wheel, expressed in $\mathrm{mm}^3/\mathrm{mm}^2$. After the track integration, we sum the contact points of each wheel:

$$\sum_{i=1}^{N_{PDC}} \Delta_{P^{jk}_{wi}}(s_w) = \Delta^{jk}_{w}(s_w) \tag{25}$$

where N_{PDC} is the maximum number of contact points of each single wheel rail pair. Since the number of contact points is usually less than N_{PDC} and changes in time during the dynamic simulation, the amount of worn material related to non-active contact points is automatically set equal to zero.

$$\sum_{k=1}^{N_c} p_k \frac{1}{N_w} \sum_{j=1}^{N_w} \Delta_{P^{jk}_{w}}(s_w) = \bar{\Delta}_w(s_w) \tag{26}$$

where N_c is the number of the simulated railway curved segments; N_w is the number of the wheelsets for the vehicle; p_k is the weighting factor of the kth curve derived from the statistical analysis.

Assuming that, inside each discrete unit, the wear quantity is close to linear with the travelled distance. This requires the unit length small enough to neglect the profile variation between two consequent units. In this way, the total length is discretized by a series of unit lengths, and each unit length is discretized by a series of track lengths. Mark the total mileage of the worn vehicle as total length km_{tot}, the unit length inside each discrete unit as km_{unit}, and the track length for each simulation inside one unit as l_{track}. Fig. 4 illustrates the discretization of the total mileage. It is possible to amplify the removed material during the dynamic simulations by means of a scaling factor which increases the distance travelled by the vehicle.

An adaptive approach is applied for updating the wheel and rail profiles:

$$\bar{\Delta}^{w}(s_w)\frac{km_{step}}{l_{track}} = \bar{\Delta}^{wsc}(s_w) \tag{27}$$

where km_{step} is calculated in an adaptive way setting a threshold value D^{w}_{step} on the maximum of the removed material quantity on the wheel at each discrete step:

$$km_{step} = l_{track}\frac{D^{w}_{step}}{max(\bar{\Delta}^{w}_{j}(s_w))} \tag{28}$$

where $max(\bar{\Delta}^{w}_{j}(s_w))$ corresponds to the maximum value of wear depth obtained from the simulation before the scaling operation.

The approach imposes a threshold value on the maximum of the removed material at each discrete step of the procedure. The evaluation of the discrete steps, represents the major difference between the update strategy of wheel and rail. It fits well in following the behaviour of the wear evolution that could present non-linear characteristics outside the discrete steps. The smoothing of the removed material function is necessary to remove the numerical noise that affects this quantity and that would be passed to the new profile of wheel and rail causing problems to the global contact model.

$$\Gamma[\bar{\Delta}^{wsc}(s_w)] = \bar{\Delta}^{wsc}_{sm}(s_w) \tag{29}$$

where Γ is the interpolation function. In this paper, we apply a spline interpolation function method to smooth. Eventually, the updated profiles can be obtained.

$$\begin{pmatrix} y_w(s_w) \\ w_o(s_w) \end{pmatrix} - \bar{\Delta}^{wsc}_{sm}(s_w)\vec{\mathbf{n}}^{r}_{w} = \begin{pmatrix} y_w(s_w) \\ w_n(s_w) \end{pmatrix} \tag{30}$$

3. Results

This section firstly introduces the comparison of wheel profile evolution between the simulated and the measured cases. After the validation of the proposed wear prediction model, a sensitivity analysis will be presented. Different cases with various stiffness of fastener and rail-pad system have been submitted for wear predicting simulation. The influence on wear prediction from the track flexibility are discussed finally.

3.1. Validation

With the proposed model, wear prediction for the wheel profile is performed. The simulated results are then compared with evolution of the vehicle running on Wuhan–Guangzhou high speed railway line. The vehicle model and track model in current work are based on the CRH2 EMU vehicle and the CRTS I slab track (Fig. 5), where the maximum running speed is 350 km/h. The types of the wheel and the rail profile in this case are the standard LMA and CN60 profiles, as illustrated in Fig. 6. Parameters of the CRH2 high speed vehicle and the slab track can be referred in [35].

The most worn wheel is selected for analysis, as is presented in Fig. 7, the measured wear profiles along 83,000 km, 132,000 km, 169,000 km, 192,000 km and the standard profile show the distribution of the wear along the wheel thread and the flange for different travelling distance. The measured wear depth of the wheel profiles along different travelling distance is shown in Fig. 8.

The wear evolution on the wheel profile from the experiment shows that the main worn region locates in the −20 to 25 mm range around the nominal rolling circle, and secondly in the −30 to −40 mm range around the flange. The depth of wear is close to 0.35 mm at the running distance of 83,000 km. The maximum depth of wear reaches around 0.7 mm at a running distance of 192,000 km. The wear rate of the profile at the initial phase, 0–83,000 km is larger than the later phase 83,000–192,000 km.

The field measurements are applied for validation of the wear prediction model proposed in this paper. To describe the railway line track layout, a statistical approach has been used to reduce the total computational effort. In current simulation, the track is represented by a group of lines with different radius, including R2500 m, R3000 m, R5000 m, R6500 m, R7000 m, R8000 m, R9000 m, R10000 m and the tangential line as listed in 2.

The threshold value on the maximum thickness of material removed by wear on the wheels at each wheel step D^{w}_{step} is assigned as 0.1 mm.

Figs. 9 and 10 show the evolution and the wear depth of the wheel profiles from the wear prediction model. Note that the most worn wheel among all is selected here to be shown.

(a) CRH2C high-speed EMU

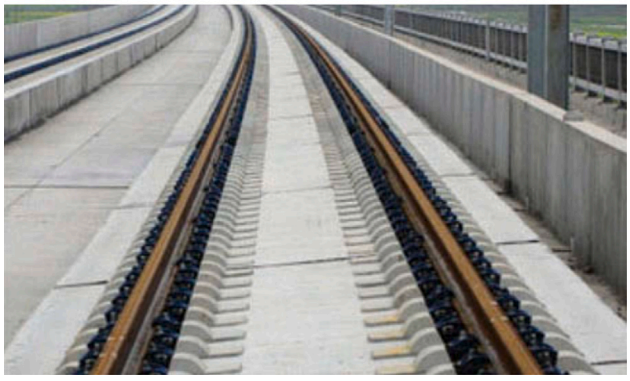

(b) CRTS-I non-ballasted track

Fig. 5. Wuhan to Guangzhou high speed railway line: train and track.

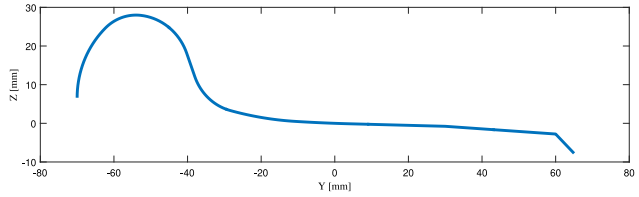

(a) LMA wheel profile

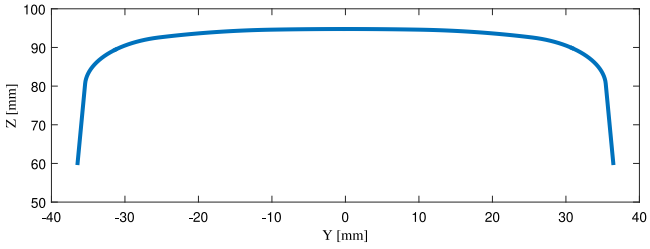

(b) CN60 rail profile

Fig. 6. Profiles of wheel and rail.

It can be seen from Figs. 9 and 10 that the wear distribution from the field measurements is well reflected in the simulated results. The main worn regions include firstly the wear thread around −20 to 25 mm from the nominal rolling circle, and then −30 to −50 mm range around the flange. The comparison of wear depth as the running distance can is illustrated in Fig. 11. It is clear that the wear of wheel get developed quicker in the initial phase (0–10,000 km) than that of later phase.

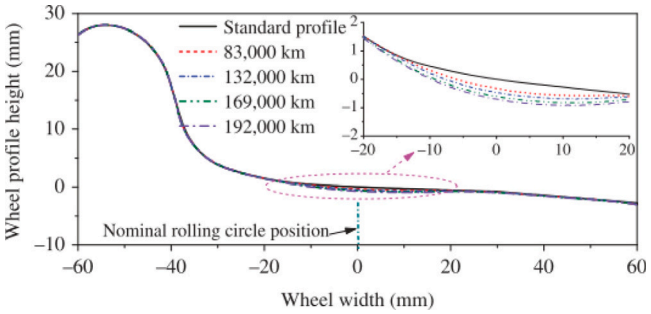

Fig. 7. Evolution of wheel profiles from experiments [35].

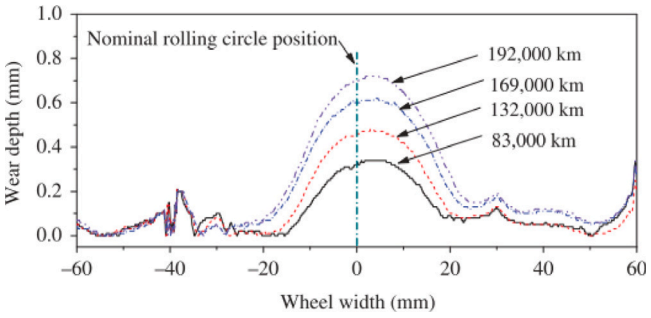

Fig. 8. Wear depth of wheel profiles from experiments [35].

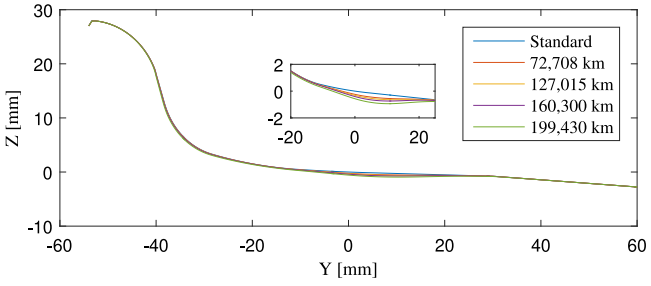

Fig. 9. Evolution of wheel profiles from simulation.

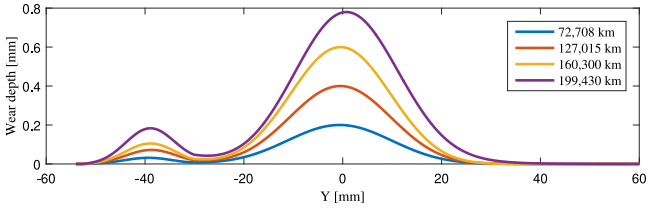

Fig. 10. Wear depth of wheel profiles from simulation.

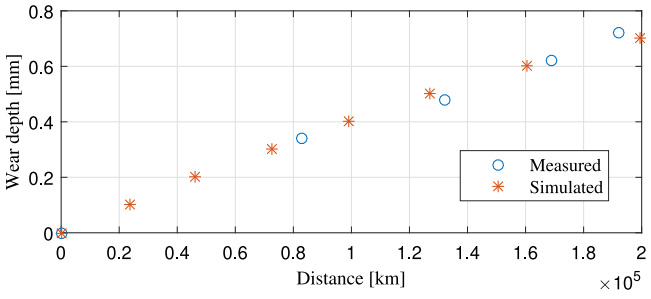

Fig. 11. Comparison of wheel wear evolution between simulated and measured results.

Table 2
Track layout of the high speed railway line for simulation.

Curve radius [m]	Vehicle speed [km/h]	Percentage [%]
2500	200	0.40
3500	200	0.28
5500	200	0.96
6000	200	0.23
7000	300	0.73
8000	300	2.79
9000	300	11.84
10000	300	10.93
>10000	300	71.84

Table 3
The values of railpad stiffness under different cases.

Cases	Case 1	Case 2	Case 3	Case 4	Case 5
Lateral raildpad stiffness [MN/m]	3	6	15	**30**	60
Vertical railpad stiffness [MN/m]	1.5	3	7.5	**15**	30

3.2. Sensitivity analysis

In order to investigate the influence of the railpad stiffness on the wheel wear evolution, the sensitivity analysis is performed. To simplify the simulation condition, one curved track with 6000 m radius, instead of the full track represented by different radii is investigated. The rail cant is 1/40 for both left and right rail, while the super-elevation is 80 mm. The vehicle operating speed is 250 km/h, and the frictional coefficient between the wheel and the rail is 0.35.

A series of different values of the railpad stiffness are set in Table 3. Note that the Case 4 corresponds to the standard value. For each case, the fixed step length of the wear evolution D^{w}_{step} is assigned as 0.1 mm. Eight updating steps are taken into consideration.

The simulated results under 5 different cases are shown from Figs. 12 to 15, including the wear depth evolution (Fig. 12), the wheel–rail contact location (Fig. 13), the running distance (Fig. 14), and the wheel–rail contact force (Fig. 15). In each sub-figure of Fig. 12, the X-axis represents the lateral position of the contact point relative to the nominal circle of the wheel, and the Y-axis represents the value of wear depth; in each sub-figure of Fig. 13, the X-axis represents time histories, and the Y-axis represents the lateral position of the contact point relative to the nominal circle of the wheel.

The influence of railpad stiffness on wear distribution can be observed from Figs. 12 and 13. For all 5 cases, the peak of the wear depth is found near 15 mm to the nominal rolling circle. As the wear develops, when the stiffness is different, the peaks of the wear depth goes differently, that when the stiffness is lower, the wear is found less concentrated. For Case 1 with lowest stiffness, the wear develops towards the nominal rolling circle and further beyond. For the Cases 2, 3 and 4, the wear develops only slowly towards the nominal rolling circle. Results of Case 5 show a significantly different performance. The peaks of wear depth are found one near nominal wheel circle, and one around 15 mm from there.

Above difference on wear distribution is significantly related to the wheel–rail contact location at each step for all cases, shown in Fig. 13. The wear initially appears about 15 mm near the nominal rolling circle, and then develops towards the nominal rolling circle. When the stiffness is lower than the standard case, the wear location reaches the flange easier. Namely, higher flexibility of the track system leads to the wear distribution closer to the flange.

Fig. 14 shows the running distance in different cases with the change of updating step. The effect of railpad stiffness on wheel–rail contact force is shown in Fig. 15, including the vertical and lateral directions. It is seen that, for the cases with lower stiffness, the running distance is higher than that of the standard case. This could be contributed from the wheel–rail contact force variation, as shown in

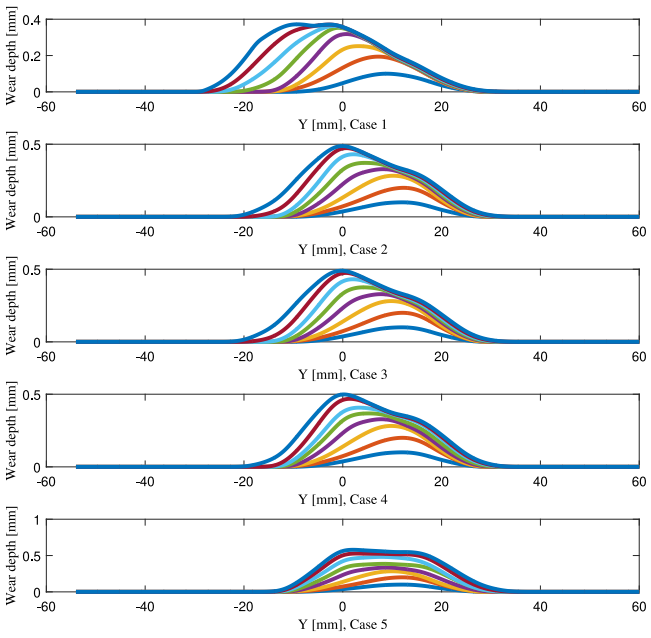

Fig. 12. Comparison of wheel wear evolution among different simulation cases.

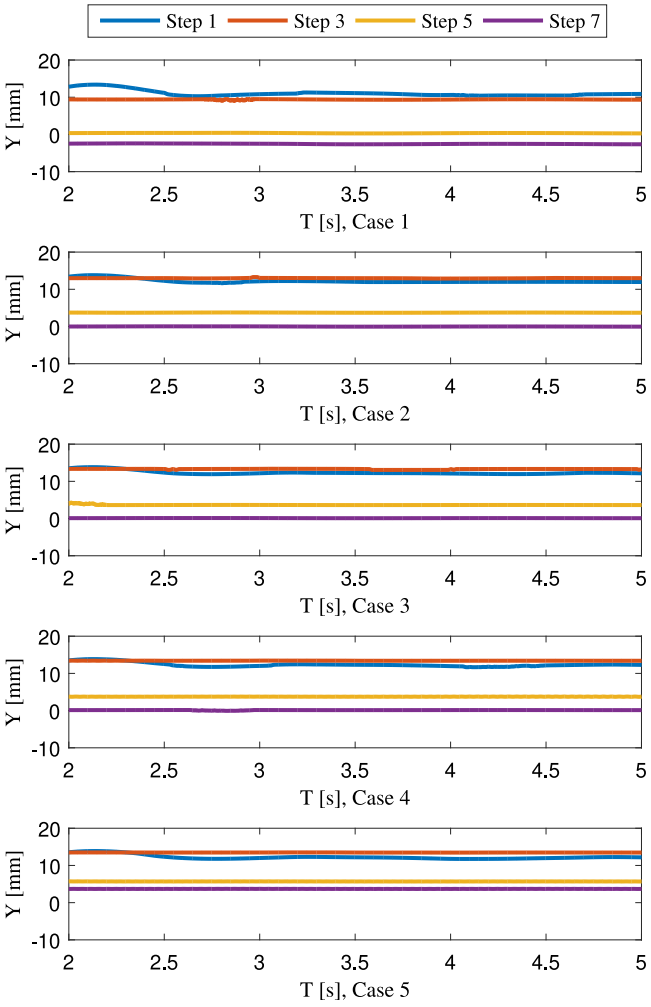

Fig. 13. Comparison of wheel–rail contact location at different steps among different simulation cases.

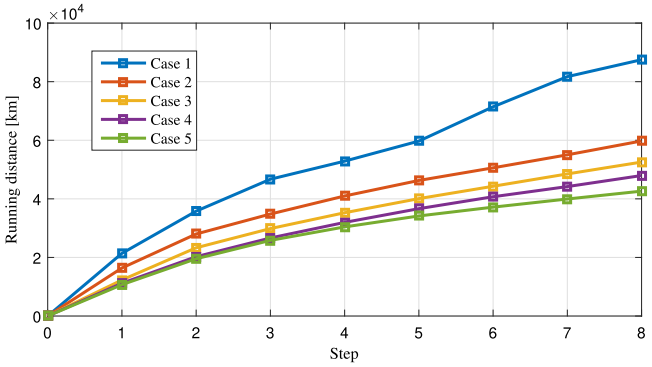

Fig. 14. Comparison of running distance among different simulation cases.

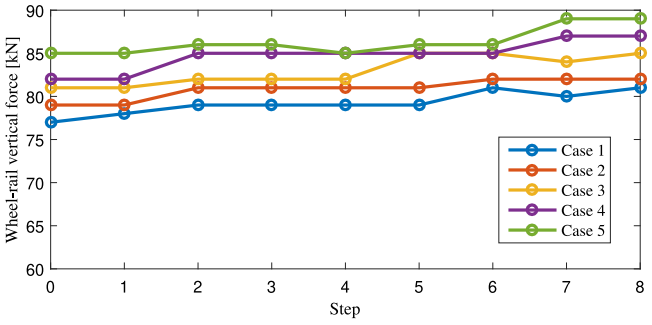

(a) Wheel-rail vertical force

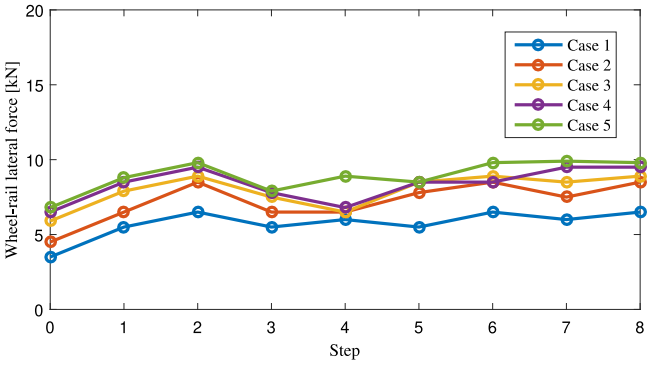

(b) Wheel-rail lateral force

Fig. 15. Wheel–rail contact forces for difference cases.

Fig. 15. When the railpad stiffness is lower, the wheel–rail contact forces are relatively lower, which leads to a slower wear occurrence.

Overall, higher flexibility of the track system extends the running distance that the wheel can resist.

4. Conclusions and future work

A new model for predicting wheel profile wear has been studied in this paper. The model adopts the vehicle–track coupled model for dynamics simulation, and the local contact model for contact variables calculation, and an energetic approach for surface wear evaluation. By introducing a multilayer track model, the wear prediction model is able to consider the effect of track flexibility on wear evolution.

The simulation of the wheel and rail wear of the high speed vehicle running on the slab track was performed, adopting the statistical approach to represent the entire line. And the wheel profile evolution was compared to that from field measurements. The results from simulation are in well consistence with those from field measurements, that the distribution of the wear and the depth along travelling distance are both well matched. With the validated wear prediction model, an investigation on the influence of the railpad stiffness on wear evolution. The analysis show that the railpad stiffness affects both the distribution and the depth of the wear significantly. Higher stiffness results in a more concentrated distribution of wheel–rail contact points, and finally affects the wear distribution. Higher flexibility of the track system leads to both lower vertical and lateral wheel–rail contact forces, and in this way it affects the running distance of the wheel. The wear develops slower when the stiffness is lower than the standard case.

In the future research, an improved wear prediction model will consider the evolution of the rail. New test cases for different railway lines will be concerned as well. Based on the validated model, more investigations on the track flexibility influencing the wear for different railway applications will be conducted.

Declaration of competing interest

The authors declare that they have no known competing financial interests or personal relationships that could have appeared to influence the work reported in this paper.

Acknowledgements

This research did not receive any specific grant from funding agencies in the public, commercial, or not-for-profit sectors.

References

[1] J. Archard, Contact and rubbing of flat surfaces, J. Appl. Phys. 24 (8) (1953) 981–988.
[2] R. Luo, H. Shi, W. Teng, C. Song, Prediction of wheel profile wear and vehicle dynamics evolution considering stochastic parameters for high-speed train, Wear 392 (2017) 126–138.
[3] T. Pearce, N. Sherratt, Prediction of wheel profile wear, Wear 144 (1–2) (1991) 343–351.
[4] I. Zobory, Prediction of wheel-rail profile wear, Veh. Syst. Dyn. 28 (2–3) (1997) 221–259.
[5] T. Jendel, Prediction of wheel profile wear comparisons with field measurements, Wear 253 (1–2) (2002) 89–99.
[6] T. Jendel, M. Berg, Prediction of wheel profile wear: methodology and verification, Veh. Syst. Dyn. 37 (sup1) (2002) 502–513.
[7] R. Enblom, M. Berg, Simulation of railway wheel profile development due to wear influence of disc braking and contact environment, Wear 258 (7–8) (2005) 1055–1063.
[8] R. Lewisa, R. Dwyer-Joyce, Wear mechanisms and transitions in railway wheel steels, Proc. Inst. Mech. Eng. J 218 (6) (2004) 467–478.
[9] R. Lewis, U. Olofsson, Mapping rail wear regimes and transitions, Wear 257 (7–8) (2004) 721–729.
[10] R. Lewis, F. Braghin, A. Ward, S. Bruni, R. Dwyer-Joyce, K. Bel Knani, P. Bologna, Integrating dynamics and wear modelling to predict railway wheel profile evolution, 2003.
[11] J. De Arizon, O. Verlinden, P. Dehombreux, Prediction of wheel wear in urban railway transport: comparison of existing models, Veh. Syst. Dyn. 45 (9) (2007) 849–866.
[12] J. Pombo, J. Ambrosio, M. Pereira, R. Lewis, R. Dwyer-Joyce, C. Ariaudo, N. Kuka, Development of a wear prediction tool for steel railway wheels using three alternative wear functions, Wear 271 (1–2) (2011) 238–245.
[13] B. Peng, S. Iwnicki, P. Shackleton, D. Crosbee, Comparison of wear models for simulation of railway wheel polygonization, Wear 436 (2019) 203010.
[14] G. Tao, Z. Wen, X. Jin, X. Yang, Polygonisation of railway wheels: a critical review, Railway Eng. Sci. (2020) 1–29.
[15] E. Butini, L. Marini, M. Meacci, E. Meli, A. Rindi, X. Zhao, W. Wang, An innovative model for the prediction of wheel-rail wear and rolling contact fatigue, Wear 436 (2019) 203025.
[16] X. Jin, Z. Wen, X. Xiao, Z. Zhou, A numerical method for prediction of curved rail wear, Multibody Syst. Dyn. 18 (4) (2007) 531–557.
[17] G.-q. Tao, X. Du, H.-j. Zhang, Z.-f. Wen, X.-s. Jin, D.-b. Cui, Development and validation of a model for predicting wheel wear in high-speed trains, J. Zhejiang Univ. Sci. A 18 (8) (2017) 603–616.
[18] X. Li, X. Jin, Z. Wen, D. Cui, W. Zhang, A new integrated model to predict wheel profile evolution due to wear, Wear 271 (1–2) (2011) 227–237.

[19] X. Li, T. Yang, J. Zhang, Y. Cao, Z. Wen, X. Jin, Rail wear on the curve of a heavy haul line numerical simulations and comparison with field measurements, Wear 366 (2016) 131–138.
[20] M. Ignesti, M. Malvezzi, L. Marini, E. Meli, A. Rindi, Development of a wear model for the prediction of wheel and rail profile evolution in railway systems, Wear 284 (2012) 1–17.
[21] J.F. Aceituno, P. Wang, L. Wang, A.A. Shabana, Influence of rail flexibility in a wheel/rail wear prediction model, Proc. Inst. Mech. Eng. F 231 (1) (2017) 57–74.
[22] G. Tao, D. Ren, L. Wang, Z. Wen, X. Jin, Online prediction model for wheel wear considering track flexibility, Multibody Syst. Dyn. 44 (3) (2018) 313–334.
[23] I. Kaiser, G. Poll, J. Vinolas, Modelling the impact of structural flexibility of wheelsets and rails on the wheel-rail contact and the wear, Wear (2020) 203445.
[24] A. Khajehdezfuly, Effect of rail pad stiffness on the wheel/rail force intensity in a railway slab track with short-wave irregularity, Proc. Inst. Mech. Eng. F 233 (10) (2019) 1038–1049.
[25] W. Zhai, Vehicle-Track Coupled Dynamics: Theory and Applications, Springer, Singapore, 2020.
[26] W. Zhai, K. Wang, C. Cai, Fundamentals of vehicle–track coupled dynamics, Veh. Syst. Dyn. 47 (11) (2009) 1349–1376.
[27] K. Wang, The track of wheel contact points and the calculation of wheel/rail geometric contact parameters, J. Southwest Jiaotong Univ. 1 (10) (1984) 89–98.
[28] J.J. Kalker, On the rolling contact of two elastic bodies in the presence of dry friction, 1967.
[29] Z. Shen, J. Hedrick, J. Elkins, A comparison of alternative creep force models for rail vehicle dynamic analysis, Veh. Syst. Dyn. 12 (1–3) (1983) 79–83.
[30] S. Zhu, C. Cai, Interface damage and its effect on vibrations of slab track under temperature and vehicle dynamic loads, Int. J. Non-Linear Mech. 58 (2014) 222–232.
[31] J. Kalker, A fast algorithm for the simplified theory of rolling contact, Veh. Syst. Dyn. 11 (1) (1982) 1–13.
[32] O. Polach, Creep forces in simulations of traction vehicles running on adhesion limit, Wear 258 (7–8) (2005) 992–1000.
[33] M. Meacci, Z. Shi, E. Butini, L. Marini, E. Meli, A. Rindi, A local degraded adhesion model for creep forces evaluation: An approximate approach to the tangential contact problem, Wear 440 (2019) 203084.
[34] F. Braghin, R. Lewis, R. Dwyer-Joyce, S. Bruni, A mathematical model to predict railway wheel profile evolution due to wear, Wear 261 (11–12) (2006) 1253–1264.
[35] W. Zhai, P. Liu, J. Lin, K. Wang, Experimental investigation on vibration behaviour of a *CRH* train at speed of 350 km/h, Int. J. Rail Transp. 3 (1) (2015) 1–16.